RSC Advances

RSC Publishing

PAPER

View Article Online
View Journal | View Issue

Synthesis and self-assembly of triphenylene-containing conjugated macrocycles†

Cite this: *RSC Advances*, 2013, **3**, 6008

Tanmoy Dutta,[a] Yanke Che,[b] Haizhen Zhong,[c] John H. Laity,[d] Vladimir Dusevich,[e] James B. Murowchick,[f] Ling Zang[b] and Zhonghua Peng*[a]

Received 20th December 2012,
Accepted 11th February 2013

DOI: 10.1039/c3ra23421e

www.rsc.org/advances

Two imine-based shape-persistent macrocycles containing triphenylene building blocks, along with their noncyclic model compounds, have been synthesized. Their stable conformations are predicted by quantum mechanical calculations and confirmed by 2D NOESY NMR measurements. Compared to the noncyclic model compounds, the macrocycles (**3** and **6**) show a higher propensity for solution self-assembly due to their stronger π–π stacking interactions, and form micro-objects which exhibit an enhanced conductivity after doping. While both macrocycles have identical molecular geometries and very similar structures, their solution self-assembly leads to micro-objects with very different shapes. The two macrocycles also show different pH-dependent optical properties.

Introduction

Shape-persistent macrocycles (SPMs) based on π-conjugated systems appeal to scientists from both fundamental research aspects and applied technology fronts.[1] Driven mostly by π–π stacking interactions, these electrically active macrocycles can self-assemble to form molecular crystals with wide channels.[2] Among the reported SPMs, those containing polycyclic aromatic systems (PCAs) are particularly interesting due to their high propensity for strong π–π stacking aggregation and the associated appealing electronic and optical properties of these stacked PCAs.[3] For example, π-stacked columns of some PCAs exhibit strong electron delocalization and a high charge-mobility.[4] PCA-containing SPMs can self-assemble to form multiple PCA-stacked columns which can facilitate charge transport, a property crucial to some molecular electronic devices such as light-emitting diodes, field-effect transistors, solar cells and sensors.[4,5] Indeed, PCAs such as carbazoles, triphenylenes *etc.*, have been incorporated into SPMs,[6] some of which have been found to self-assemble into nanofibers with sizable conductivity along their long axis.[7] Although these studies are exemplary, SPMs containing PCAs are still rare, presumably due to the synthetic challenges associated with the preparation of size-selective macrocycles. We have been interested in preparing conjugated systems containing PCAs, including conjugated macrocycles,[8] dendrimers[9] and polymers.[10] In this communication, we report the synthesis and self-assembly of two triphenylene-containing conjugated macrocycles. The two macrocycles, differing only in the positions of the imine N atoms, show dramatically different optical properties and self-assemble into different microstructures.

[a]*Department of Chemistry, University of Missouri-Kansas City, Kansas City, MO 64110, United States. E-mail: pengz@umkc.edu; Fax: +1-816-235-2290; Tel: +1-816-235-2288*
[b]*Department of Materials Science & Engineering, University of Utah, Salt Lake City, UT 84108, United States*
[c]*Department of Chemistry, University of Nebraska-Omaha, Omaha, NE, United States*
[d]*Department of Cell Biology and Biophysics, University of Missouri-Kansas City, Kansas City, MO 64110, United States*
[e]*Department of Oral Biology, University of Missouri-Kansas City, Kansas City, MO 64110, United States*
[f]*Department of Geosciences, University of Missouri-Kansas City, Kansas City, MO 64110, United States*

† Electronic supplementary information (ESI) available: supplementary data associated with this article can be found in the online version. The data includes ^{1}H and ^{13}C NMR, MALDI-TOF spectra, 2D NOESY spectra, X-ray diffraction patterns of the self-assembled structures and QM calculations. See DOI: 10.1039/c3ra23421e

Results and discussion

Synthesis

Scheme 1 shows the structures and syntheses of the two triphenylene-containing macrocyles **3** and **6**. Except for the location difference of the four imine nitrogen atoms, the two macrocycles have an identical structure. The triphenylene derivative **1** was synthesized in good yield *via* a previously published procedure.[11] The two bromo groups in **1** were converted to aldehydes *via* a lithium–halogen exchange followed by quenching with excess DMF. The synthesis of the model compound **3m** was afforded *via* a condensation reaction of **2** with freshly distilled aniline in the presence of molecular sieves and a Dean–Stark trap. The same reaction conditions were utilized to synthesize macrocycle **3** *via* the reaction of **2** with *m*-diaminobenzene.

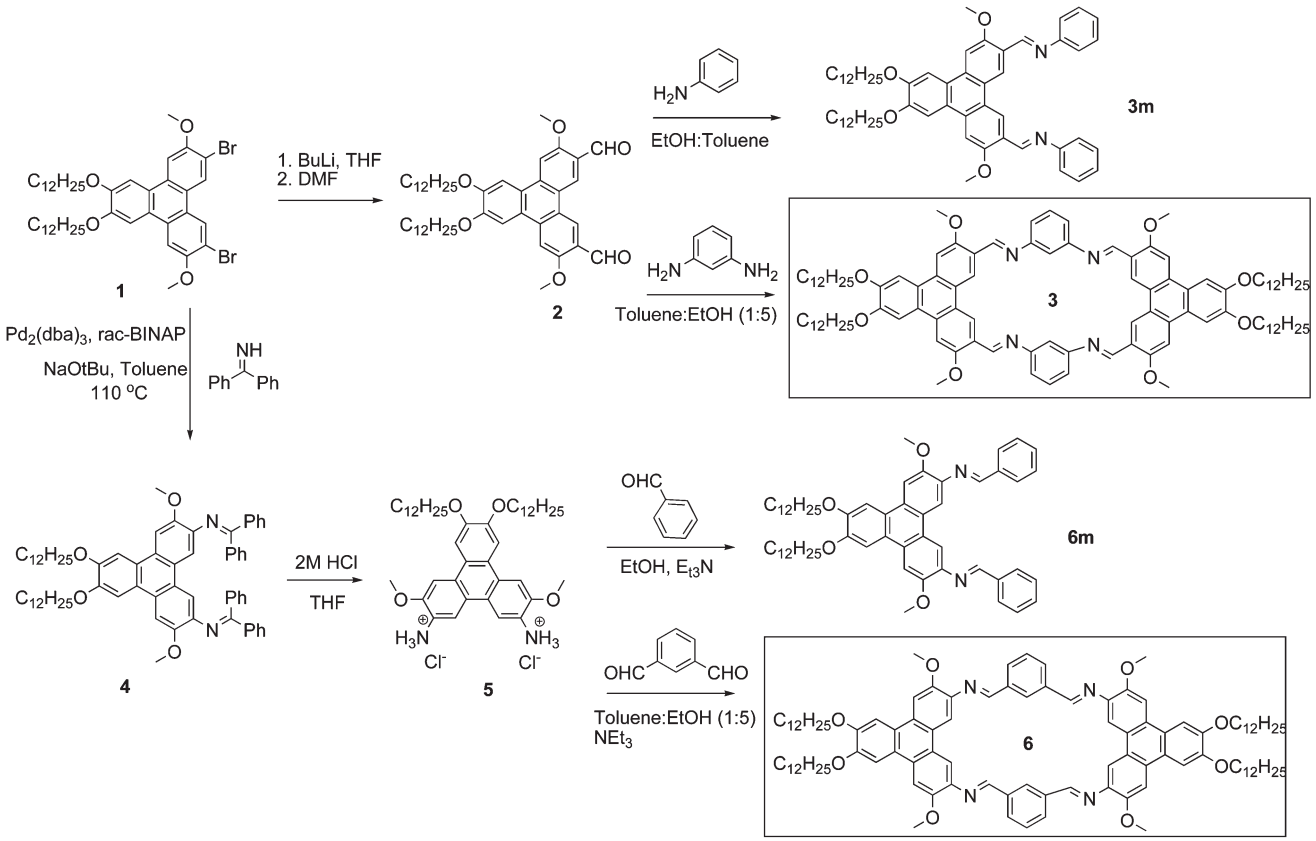

Scheme 1 The synthesis of macrocycles **3** and **6** and their model compounds **3m** and **6m**.

To synthesize macrocycle **6**, compound **1** was first converted to compound **4** through a Pd-catalyzed coupling reaction.[12] The acid-catalyzed hydrolysis of **4** yielded a triphenylene derivative **5**, with two amino functional groups in the salt form. The condensation reaction of **5** with benzaldehyde or isophthalaldehyde afforded the model compound **6m** and the macrocycle **6**, respectively. Both macrocyles **3** and **6** are soluble in common organic solvents and their structures are confirmed by ^{1}H NMR, MALDI-TOF and elemental analysis (see experimental section and ESI† for detailed characterization data).

Conformation analysis

An imine bond may exist as a *cis* or *trans* isomer. However, due to geometrical constraints, it is likely that the imine bonds in **3** and **6** adopt only the *trans* conformation. Depending on the orientation of the imine-H's, the macrocycle **3** (or **6**) may adopt $\mathbf{3_i}$ (or $\mathbf{6_i}$, all imine H's pointing towards the ring cavity), $\mathbf{3_o}$ (or $\mathbf{6_o}$, all imine H's pointing away from the ring cavity), or $\mathbf{3_{io}}$ (or $\mathbf{6_{io}}$ two inside and two outside) structures, as shown in Fig. 1. These configurations can interconvert through rotations along the two parallel single bonds that are indicted by arrows in Fig. 1. Whether an imine H is located inside or outside the ring cavity can be determined by its physical proximity to H7 or H5.

To determine which isomer compounds **3** and **6** might adopt, we carried out 2D ^{1}H–^{1}H NOESY experiments. As shown in Fig. 2a, the imine hydrogen H2 (9.34 ppm) has a strong NOE contact with H7 (7.33 ppm) and H9 (4.21 ppm) but a negligible NOE contact with H5, indicating that **3** adopts mostly the $\mathbf{3_o}$ conformation.[13] On the other hand, the 2D ^{1}H–^{1}H NOESY spectrum of **6** (Fig. 2b) shows that the imine hydrogen H2 has NOE contacts with H5 and H1, but not H7, indicating that, contrary to **3**, the imine H's in **6** are located inside the ring cavity. In other words, **6** adopts a $\mathbf{6_i}$ conformation. It is noted that the $\mathbf{3_o}$ and $\mathbf{6_i}$ conformations have an identical molecular shape, although their imine H atoms point in opposite directions.

Quantum mechanics calculations

To provide a reasonable explanation of why one isomer is preferred over another, we carried out quantum mechanics (QM) calculations for compounds **3** and **6**. To simplify the calculations, we truncated $-OC_{12}H_{25}$ to $-OC_2H_5$. This simplification is justifiable because (a) the superimposition of **3** and **6** with $-OC_{12}H_{25}$ and their counterparts with $-OC_2H_5$ showed that the core macrocycle structures were almost identical (Fig. S20†), and (b) the change was far from the imine hydrogen and therefore should have little effect on the core geometry.

DFT calculations with the basis set B3LYP/6-31G**//B3LYP/STO-3G show that $\mathbf{3_o}$ is indeed the most stable conformer (Table 1). The other two isomers of **3** ($\mathbf{3_{io}}$ and $\mathbf{3_i}$) are at least 11 kcal mol^{-1} higher in energy than $\mathbf{3_o}$, suggesting that at room temperature, $\mathbf{3_o}$ would be the dominant conformer. $\mathbf{6_i}$ is also calculated to be the most stable conformer. However, the

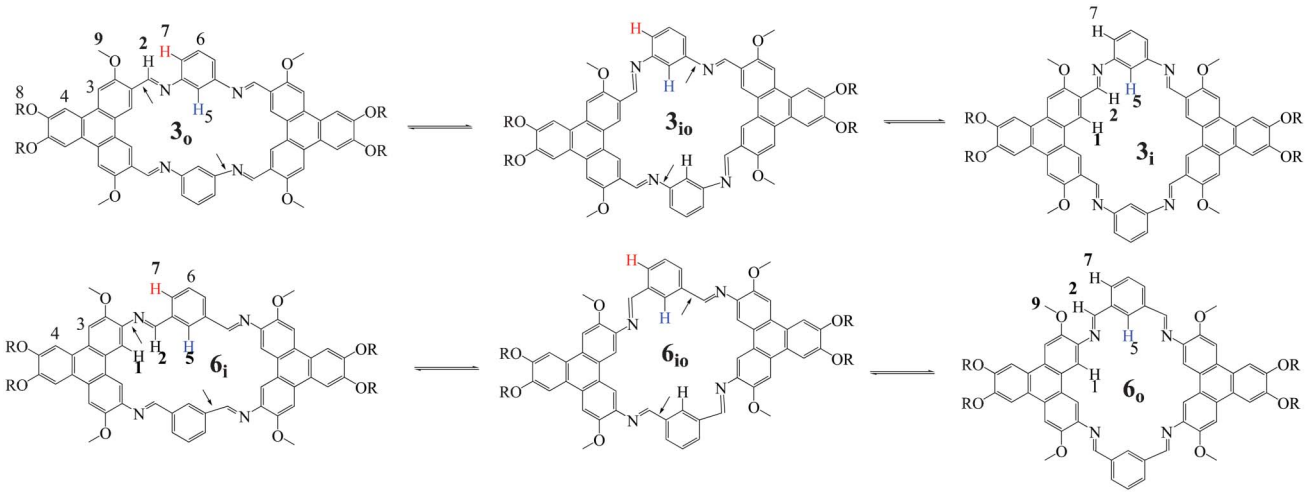

Fig. 1 Various conformers of macrocycles **3** and **6** and their interconversion.

energetic difference between conformers of **6** is much smaller compared to those of **3**. The experimental observations of $\mathbf{6_i}$ indicate that the inter-conversion between the conformers is kinetically hindered. The high rotational barrier is likely due to 1) the rigidity of the macrocyclic skeleton, 2) the requirement of simultaneous rotation along two bonds, and 3) the partial double bond character of the rotating C–C and C–N bonds (indicated by arrows in Fig. 1) due to extended π-conjugation. Therefore, $\mathbf{3_o}$ and $\mathbf{6_i}$ are the preferred products during the imine/macrocycle formation process. The selectivity may be explained as shown in Fig. 3. The protonated hemiaminal intermediates leading to $\mathbf{3_o}$ and $\mathbf{6_i}$ are likely to be thermodynamically more stable than other intermediates due to the existence of hydrogen bonding.

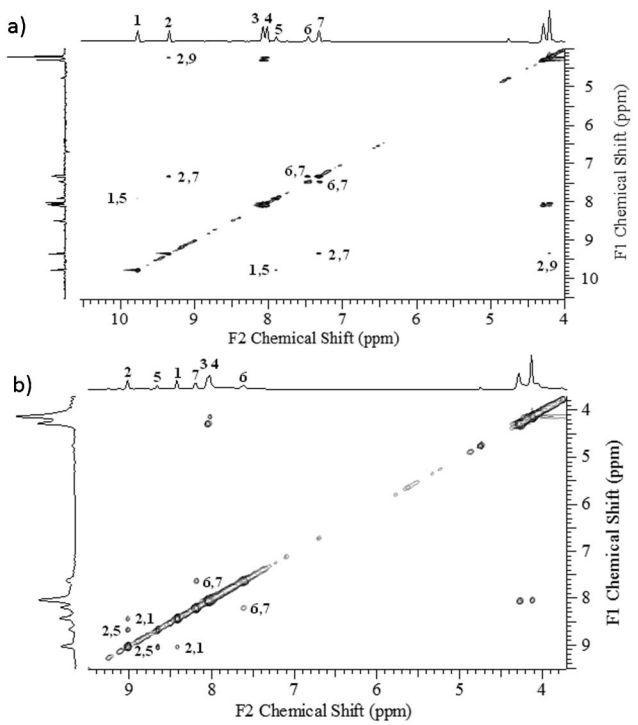

Fig. 2 Selected regions from a 2D 600 MHz ^{1}H NMR watergate NOESY spectra of **3** (a) and **6** (b), showing strong NOE contacts, recorded in THF-*d8* at 298 K with a 400 ms NOE mixing time.

Optical properties

Both **3** and **6** are soluble in THF under ambient conditions, but are insoluble in methanol and hexane. In THF, macrocycle **3** shows three absorption bands at 298, 360 and 414 nm, and a shoulder band at around 390 nm (Fig. 4). Compared to the model compound **3m**, which also shows these bands, and a 5–10 nm bathochromic shift is observed for all bands. Macrocycle **6** and its model compound **6m**, on the other hand, show only two broad absorption bands at around 280 nm and 365 nm for **6** and 275 nm and 355 nm for **6m**. While the absorption tails for both **3** and **6** extend to around 440 nm, macrocycle **3** has a much sharper band edge and better resolved vibronic features.

Macrocycle **3** and **3m** are colourless in THF, but give an orange–red solution when dissolved in $CDCl_3$. It is suspected that the residual acid in $CDCl_3$ is responsible for this colour change. To confirm the acid effect, to the THF solution of **3** (or **3m**) is added TsOH. Indeed a broad absorption extending up to 600 nm is observed for both **3** and **3m** (Fig. 5). After neutralization with Et_3N, the red-shifted band disappears and

Table 1 Ground state energies of various conformers of **3** and **6**

Conformer	Energy (hartrees)	ΔE^a (kcal mol^{-1})
$\mathbf{3_i}$	−3293.264344	23.23
$\mathbf{3_{io}}$	−3293.283739	11.06
$\mathbf{3_o}$	−3293.301365	0.00
$\mathbf{6_i}$	−3293.28764	0.00
$\mathbf{6_{io}}$	−3293.286299	0.84
$\mathbf{6_o}$	−3293.283896	2.35

^{a} Energy difference relative to the most stable conformer.

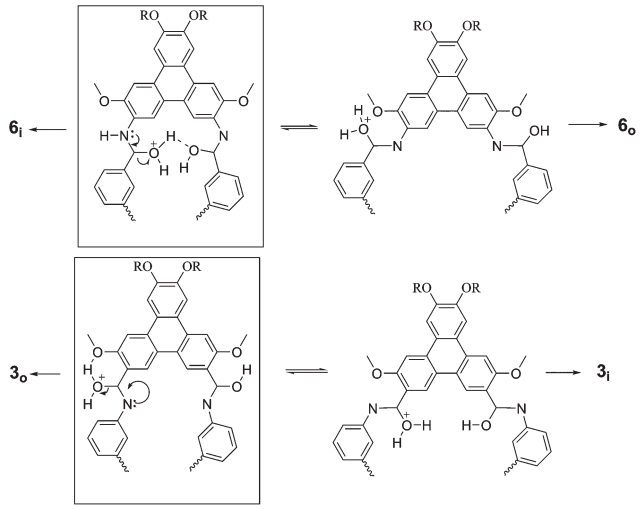

Fig. 3 Protonated hemiaminal intermediates leading to different macrocyclic conformers.

the original spectral feature in the 300–420 nm range is recovered. It is noted that, while only a slight decrease in absorbance in the 300–420 nm range occurs for **3** after the acidification/neutralization cycle, the solution of **3m** shows a significant loss in absorption in the 300–420 nm range, which is due to imine hydrolysis under acidic conditions. When the same experiment is carried out with macrocycle **6** or **6m**, a red-shifted band is not observed when acid is added. Instead, the longest absorption band (around 360 nm) completely disappeared after the addition of acid and is not recovered after subsequent neutralization, indicating that the imine bonds in **6m** and **6** have completely hydrolysed. This shows that the

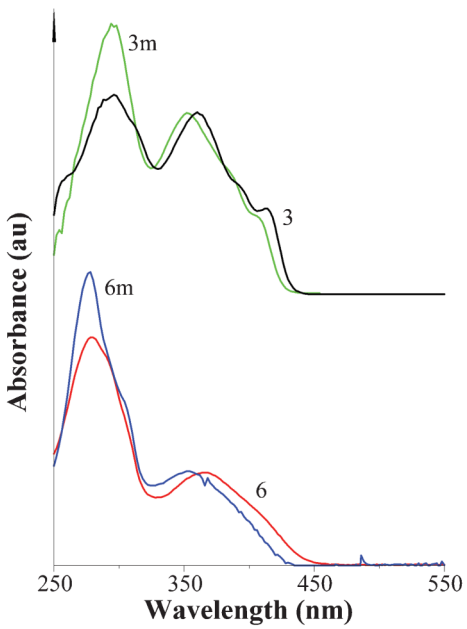

Fig. 4 The UV-Vis absorption spectra of **3m** and **3** (top), **6m** and **6** (bottom) in THF.

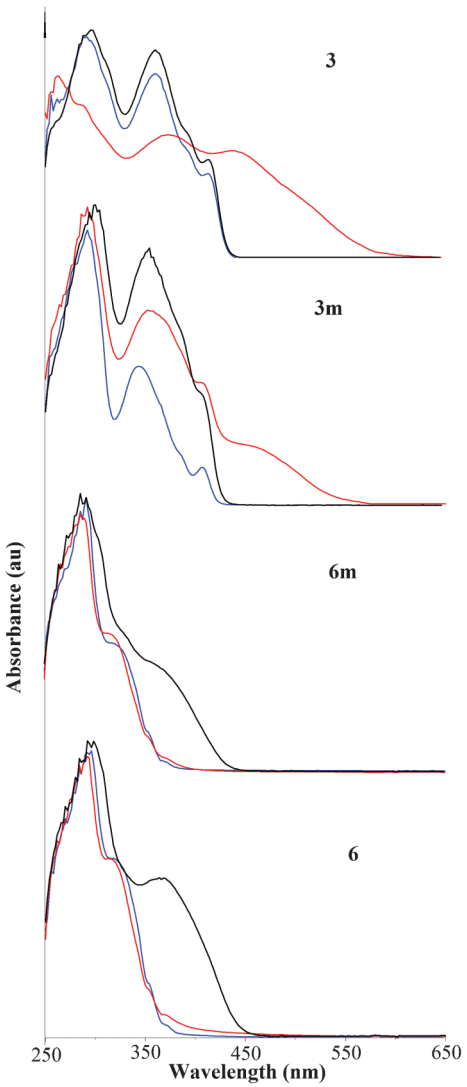

Fig. 5 The UV-Vis absorption spectra of **6**, **6m**, **3** and **3m** in original THF solution (black), after addition of TsOH (red), and after subsequent neutralization with Et_3N (blue).

imine bonds in macrocycle **3** have a higher hydrolytic stability over those in the model compound **3m** and even more so than those in **6** and **6m**. The drastically different optical properties of the two macrocycles under acidic conditions reflect their structural differences. Under acidic conditions, the imine nitrogen is protonated, which leaves the imine carbon with a partial positively charged. The adjacent electron-rich triphenylene π-system in **3** (and **3m**) helps to stabilize the carbocation through a charge transfer resonance effect (Fig. S13†). Such a charge transfer transition may account for the significantly red-shifted absorption of **3** and **3m** under acidic conditions and may also explain the better hydrolytic stability of the imine bonds in **3** and **3m**. For **6** and **6m**, imine protonation leads to a benzyl-type cation which does not have red-shifted charge transfer transitions and thus no red-shifted absorption band and exhibits a short life. The better hydrolytic stability of **3** over **3m** may be due to the rigid macrocycle

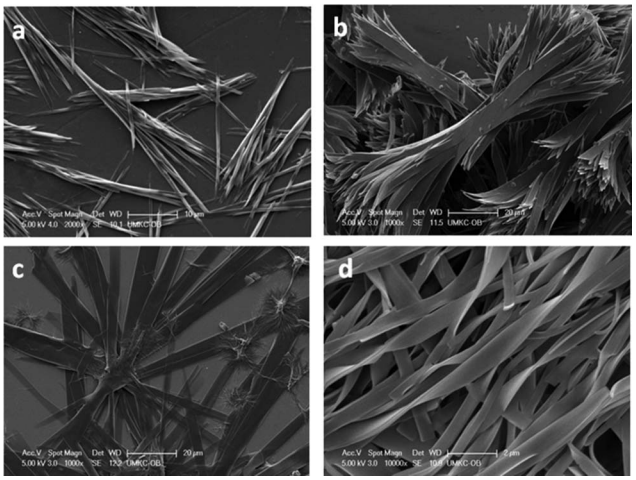

Fig. 6 SEM images of self-assembled objects from macrocycles **3** (a), **6** (b), and their model compounds **3m** (c), **6m** (d).

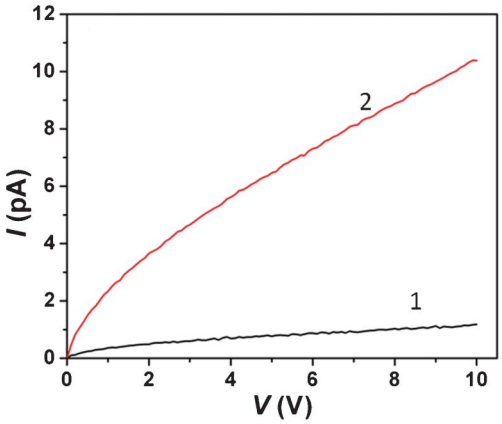

Fig. 7 *I–V* curves measured over the microfibers of **3** before (1) and after (2) being exposed to saturated iodine vapor for 5 min. The microfibers were drop cast onto a gold electrode-pair (3 μm gap, 14 μm long) fabricated on the surface of oxidized silicon.

structure which blocks the nucelophilic attack of water on the carbocation.

Solution self-assembly

When a poor solvent such as hexane or methanol is slowly diffused into the THF solution of **3** or **6**, self-assembly occurs, leading to opaque solutions in less than one day. SEM images (Fig. 6 and Fig. S14†) show that **3** self-assembles into rigid rods that are approximately 50 μm long and have an outer diameter of ~1 μm. The XRD of the fibers shows a distinct diffraction peak at 3.63 Å (Fig. S17†), which is consistent with the π–π stacking distances. Macrocycle **6**, on the other hand, self-assembles into plates/panels with dimensions of around 100 μm × 10 μm, which stack into bundles. The panels have a pointed triangular edge at the two longitudinal ends. The XRD pattern of the self-assembled plates (Fig. S18†) shows a diffraction peak at 3.42 Å, indicating a significantly shorter π–π stacking distance in **6** which is close to the graphite layer spacing of 3.35 Å. Macrocycle **6** also shows a better long range order. However, when hexane is diffused into a THF solution of **3m** or **6m**, no aggregates are visible even after 10 days. If methanol is used as the poor solvent, self-assembly does occur after four days and the SEM images show the formation of 2D ribbons (Fig. 6c and 6d). The XRD of **3m** (Fig. S19†) shows a much large π–π stacking distance of 4.17 Å. The faster self-assembly process of the macrocycles reflects their stronger π–π stacking interactions brought about by the higher number of aromatic π-systems and their relatively flat structure.

π-Stacking among triphenylene rings is believed to be responsible for the facile self-assembly of both macrocycles and the model compounds. The triphenylene stack may bring charge mobility to the assembled micro-objects. To test this hypothesis, the conductivity of the pristine microfibers of **3** with or without doping is measured. As shown in Fig. 7, the pristine fibers exhibited a minimal current of only about 1 pA under a bias of 10 V. This is consistent with the high purity of the microfibers thus fabricated. Such poor conductivity is common for single crystalline organic semiconductors. However, the microfibers demonstrated an increase in current of about one order of magnitude after exposure to saturated iodine vapor for 5 min. The enhancement in the conductivity implies not only a certain level of charge carrier doping, but more importantly efficient charge delocalization along the π–π stacking of the building block molecules (here presumably the long axis of the nanofiber).[14] To achieve a high conductivity demands both a high concentration of carriers and continuous transport pathways. The π–π stacking induced charge transport has been extensively proven for various π-conjugated molecules using both experimental and theoretical investigations.[15] Moreover, strong π–π stacking within the microfibers was also evident by the observation that the nanofibers as fabricated were completely nonfluorescent, *i.e.*, no emission was detected (using either a fluorometer or fluorescence microscope) even under high intensity of UV irradiation. However, the molecules demonstrated detectable emission when dissolved in a solution. The non-emitting phase is due to the forbidden low-energy excitonic transition as previously observed for other π-molecules.[16]

Conclusions

In summary, two shape-persistent triphenylene-based macrocycles have been synthesized. Both quantum mechanical calculations and 2D NMR measurements show that **3** adopts the $\mathbf{3_o}$ conformation and **6** adopts the $\mathbf{6_i}$ conformation. The interconversion of the conformers is restricted due to the rigid shape-persistent ring structure. Under acidic conditions, both **3** and **3m** show a significantly red-shifted absorption band which is attributed to a charge transfer transition mediated by the triphenylene π system. **6** and **6m**, on the other hand, lack such a charge transfer transition and hydrolyse rather quickly under acidic conditions. Compared to the model compounds, the macrocycles exhibit a stronger propensity for solution self-assembly. While **3** self-assembles into nano and microrods, **6**

aggregates into panels with a significantly higher crystalline order. The sizable electrical conductivity after doping and the complete fluorescence quenching of the self-assembled micro-objects indicate that strong π–π stacking among the triphenylene rings is responsible for their facile self-assembly process.

Experimental section

Solvents were distilled from appropriate drying agents under inert conditions prior to use. Unless otherwise stated, all other chemicals were purchased from commercial sources and used without further purification. All reactions were carried out under nitrogen using standard Schlenk techniques. ^{1}H NMR and ^{13}C NMR spectra were collected using a Varian INOVA 400 MHz spectrometer. 2D NOESY NMR spectra were collected using a 14.1T Varian INOVA spectrometer equipped with a cryogenically cooled probe. The NOESY spectra were collected using the Watergate NOESY pulse sequence with a mixing time of 400 ms, 16 transients and ni = 1024. Chemical shifts were referenced to residual protio-solvent signals. UV-Vis absorption spectra (10^{-6} M THF solution) were measured using a Hewlett–Packard 8452A diode array spectrophotometer. A Voyager DE Pro (Perceptive Biosystems/ABI) MALDI-TOF mass spectrometer was used for mass spectra measurements, operating in the reflector mode. Compounds were spotted for MALDI-TOF MS analysis in a matrix containing dithranol freshly dissolved in distilled THF. A field-emission scanning electron microscope (SEM) XL30 (FEI Company, Hillsboro, OR) was used with an accelerating voltage of 15.0 kV. Specimens were prepared by placing drops of suspension either on a double sided carbon tape or on a mica substrate. Specimens were used with or without sputter-coated Au–Pd. Self-assembled aggregates were obtained by the diffusion of hexane or methanol vapor through the THF solution of the respective compounds. XRD measurements were performed using a Rigaku Miniflex automated diffractometer with Cu-Kα radiation. Electrode fabrication and *I–V* measurements were done following the same procedures as previously described.[14]

Compound 1

To a solution of 2,3-bis(dodecyloxy)-6,11-dimethoxytriphenylene (2.05 g, 3.12 mmol) in 100 mL dichloromethane was added dropwise along with bromine (0.32 mL, 6.24 mmol) in 10 mL dichloromethane. The reaction mixture was stirred at room temperature for 2 h and was then poured into water. The organic layer was washed with 5% sodium thiosulphate solution and water and dried over $MgSO_4$. After removal of the solvent, the crude product was purified by recrystallization from dichloromethane/methanol to yield **1** as a yellow solid (2.0 g, 79%). ^{1}H NMR (400 MHz, $CDCl_3$) δ: 8.42 (s, 2H), 7.81 (s, 2H), 7.67 (s, 2H), 4.24 (t, J = 6.2 Hz, 4H), 4.09 (s, 6H), 1.94 (m, 4H), 1.25 (m, 36H), 0.86 (t, J = 7.2 Hz, 6H); ^{13}C NMR (100 MHz, $CDCl_3$) δ: 154.0, 149.8, 129.0, 127.4, 123.7, 122.8, 111.6, 106.8, 103.7, 69.5, 56.2, 29.7 (2), 29.6, 29.4 (2), 26.2, 22.7, 14.1; anal. calcd for $C_{44}H_{62}Br_2O_4$: C, 64.86; H, 7.67. Found: C, 64.78; H, 7.52.

Compound 2

BuLi (1.18 mL, 2.5M in hexane, 2.96 mmol) was added dropwise to a chilled solution of **1** (1.05 g, 1.28 mmol) in dry THF (90 mL) at −20 °C. The reaction mixture was stirred at −20 °C for 1 h. Then anhydrous DMF (0.397 mL, 5.15 mmol) was added dropwise. The reaction mixture was allowed to warm to room temperature overnight. After being quenched with 100 mL water, the solution was extracted with dichloromethane. The organic layer was washed twice with water, dried over $MgSO_4$, filtered and concentrated under reduced pressure. The crude product was purified by chromatography on a silica gel column using dichloromethane : hexanes (1 : 1 v/v) as the eluent, affording **2** as a yellow solid (0.71 g, 77%). ^{1}H NMR (400 MHz, $CDCl_3$) δ: 10.59 (s, 2H), 9.01 (s, 2H), 7.81 (s,2H), 7.73 (s, 2H), 4.24 (t, J = 8.0 Hz, 4H), 4.13 (s, 6H), 1.95 (m, 4H), 1.25 (m, 36H), 0.86 (t, J = 8.0 Hz, 6H); ^{13}C NMR (100 MHz, $CDCl_3$) δ: 189.5, 159.4, 150.8, 134.7, 125.1, 124.8, 124.1, 122.7, 107.6, 103.7, 69.5, 55.7, 31.9, 29.7, 29.5, 29.3, 26.2, 22.7, 14.1; anal. calcd for $C_{46}H_{64}O_6$: C, 77.49; H, 9.05. Found: C, 76.78; H, 8.90.

Compound 3m

2 (0.12 g, 0.17 mmol), molecular sieves and freshly distilled aniline (76 μL, 0.84 mmol) were added to a flask equipped with a Dean–Stark trap and reflux condenser under a nitrogen atmosphere. 10 mL anhydrous toluene and 50 mL anhydrous ethanol were added and the reaction mixture was refluxed for 2 days. After cooling to room temperature, the yellow precipitate was collected by filtration. The precipitate was washed multiple times with methanol and then hexane to yield **3m** as a yellow solid (0.09 g, 62%). ^{1}H NMR (400 MHz, THF-*d8*) δ: 9.45 (s, 2H), 9.07 (s, 2H), 8.04 (s, 2H), 7.99 (s, 2H), 7.37 (br, 4H), 7.28 (br, 4H), 7.18 (br, 2H), 4.28 (t, J = 4.8 Hz, 4H), 4.16 (s, 6H), 1.93 (m, 4H), 1.31 (m, 36H), 0.89 (t, J = 5.0 Hz, 6H); ^{13}C NMR (100 MHz, THF-*d8*) δ: 159.2, 156.3, 154.4, 151.7, 129.9, 126.4, 125.9, 125.4, 124.3, 123.5, 122.1, 108.6, 104.7, 70.1, 56.2, 33.1, 30.9, 30.7, 30.6, 23.8,14.6; MALDI-TOF MS: calcd for $C_{58}H_{74}N_2O_4$: 863.22, found: 863.22; anal. calcd for $C_{58}H_{74}N_2O_4$: C, 80.70; H, 8.64; N, 3.25. Found: C, 80.20; H, 8.83; N, 3.17.

Compound 3

To a dry flask equipped with a Dean–Stark trap, **2** (0.1 g, 0.14 mmol), *m*-phenylenediamine (0.015 g, 0.14 mmol), 10 mL anhydrous toluene, 50 mL anhydrous ethanol and molecular sieves were added. The reaction mixture was refluxed for 4 days. After cooling to room temperature, the yellow precipitate was collected by filtration. The precipitate was washed multiple times with methanol followed by hexane to yield **3** as a yellow solid (0.09 g, 40%). ^{1}H NMR (400 MHz, THF-*d8*) δ: 9.77 (s, 4H), 9.34 (s, 4H), 8.08 (s, 4H), 8.02 (s, 4H), 7.9 (br, 2H), 7.47 (br, 2H), 7.33 (br, 4H), 4.29 (t, J = 6.2 Hz, 8H), 4.21 (s, 12H), 1.94 (m, 8H), 1.32 (m, 72H), 0.9 (t, J = 5.8 Hz, 12H); ^{13}C NMR (100 MHz, THF-*d8*) δ: 159.3, 154.8, 154.7, 153.5, 151.9, 133.7, 126.2, 125.8, 124.6, 109.3, 104.8, 70.4, 57.5, 30.9, 30.8, 30.7, 30.5, 27.4, 23.7,14.5; MALDI-TOF MS: calcd for $C_{104}H_{136}N_4O_8$: 1570.21, found: 1570.21; anal. calcd for $C_{104}H_{136}N_4O_8$: C, 79.55; H, 8.73; N, 3.57. Found: C, 79.11; H, 8.84; N, 3.39.

Compound 4

A toluene solution (50 mL) of tris(dibenzylideneacetone) dipalladium(0) (0.14 g, 0.153 mmol) and *rac*-BINAP (0.19 g, 0.305 mmol) was stirred at 110 °C for 30 min under argon. After cooling to room temperature, benzophenone imine (0.26 mL, 1.55 mmol), sodium *tert*-butoxide (0.15 g, 1.55 mmol) and **1** (0.5 g, 0.614 mmol) were added to the reaction mixture and stirred at 110 °C overnight. The mixture was cooled and evaporated to dryness. The crude product was purified by column chromatography on a silica gel with ethyl acetate : hexane (1 : 3 v/v) as the eluent, affording **4** as a yellow solid (0.61 g, 97%). ^{1}H NMR (400 MHz, $CDCl_3$) δ: 7.8–7.78 (m, 4H), 7.75 (s, 2H), 7.57 (s, 2H), 7.52 (s, 2H), 7.48 – 7.38 (m, 6H), 7.15 (m, 10H), 4.16 (t, J = 6.6 Hz, 4H), 3.84 (s, 6H), 1.89 (m, 4H), 1.24 (m, 36H), 0.85 (t, J = 6.8 Hz, 6H); ^{13}C NMR (100 MHz, $CDCl_3$) δ: 170.3, 149.1, 149.0, 140.9, 139.5, 136.8, 130.7, 129.5, 128.8, 128.5, 128.1, 127.7 (2), 125.6, 123.8, 123.4, 115.0, 107.3, 103.7, 69.7, 55.6, 31.9, 29.7 (3), 29.5, 29.4 (2), 26.2, 22.7, 14.1; anal. calcd for $C_{70}H_{82}N_2O_4$: C, 82.80; H, 8.14; N, 2.76. Found: C, 82.57; H, 8.00; N, 2.69.

Compound 5

A 2.0 M HCl solution (0.7 mL, 1.4 mmol) was added dropwise to a THF solution (10 mL) of **4** (0.6 g, 0.591 mmol) at room temperature. The reaction mixture was stirred at room temperature for 1 h. The resulting precipitate was filtered and washed with hexane (10 mL × 3), dried under vacuum to yield **5** as a light yellow solid (0.4 g, 89%).^{1}H NMR (400 MHz, DMSO-*d6*) δ: 8.09 (s, 2H), 8.04 (s, 2H), 8.01 (s, 2H), 4.26 (t, J = 6.2 Hz, 4H), 4.12 (s, 6H), 3.58 (br, 4H), 1.83 (m, 4H), 1.25 (m, 36H), 0.85 (t, J = 6.8 Hz, 6H); ^{13}C NMR (100 MHz, DMSO-*d6*) δ: 149.2, 149.0, 128.3, 123.1, 122.2, 112.5, 112.3, 107.7, 104.7, 68.9, 56.1, 31.0, 28.8, 28.7, 28.6, 28.3, 25.5, 21.7, 17.4, 13.5.

Compound 6m

To a suspension of **5** (0.09 g, 0.012 mmol) in anhydrous ethanol (12 mL), triethylamine (0.08 mL, 0.573 mmol) was added. The resulting mixture was stirred at room temperature for 15 min under a nitrogen atmosphere. Molecular sieves and benzaldehyde (0.06 mL, 0.588 mmol) in anhydrous ethanol (2 mL) were then added. With a Dean–Stark trap and reflux condenser attached, the reaction mixture was refluxed for 2 days under nitrogen atmosphere. After cooling to room temperature, the yellow precipitate was collected by filtration. The precipitate was washed multiple times with methanol and then hexane to yield **6m** as a yellow solid (0.077 g, 75%). ^{1}H NMR (400 MHz, THF-*d8*) δ: 8.71 (s, 2H), 8.22 (s, 2H), 8.05 (s, 2H), 7.99 (br, 6H), 7.46 (br, 6H), 4.27 (t, J = 6 Hz, 4H), 4.06 (s, 6H), 1.92 (m, 4H), 1.31 (m, 36H), 0.9 (t, J = 6.0 Hz, 6H); ^{13}C NMR (100 MHz, THF-*d8*) δ:, 161.9, 153.0, 150.9, 143.3, 138.3, 131.9, 129.8, 129.5, 128. 8, 125.3, 124.8, 115.8, 108.4, 105.8, 70.1, 56.5, 33.1, 31.0, 30.9, 30.9, 30.8, 30.7, 30.6, 27.5, 23.8, 14.6; MALDI-TOF MS: calcd for $C_{58}H_{74}N_2O_4$: 863.22, found: 863.22; anal. calcd for $C_{58}H_{74}N_2O_4$: C, 80.70; H, 8.64; N, 3.25. Found: C, 80.13; H, 8.81; N, 3.18.

Compound 6

To a suspension of **5** (0.1 g, 0.131 mmol) in anhydrous ethanol (50 mL) and anhydrous toluene (10 mL), triethylamine (0.09 mL, 0.647 mmol) was added. The mixture was stirred at room temperature for 15 min under a nitrogen atmosphere. Molecular sieves and isophthalaldehyde (0.0176 g, 0.131 mmol) were then added and a Dean–Stark trap and reflux condenser were attached. The reaction mixture was refluxed for 4 days under a nitrogen atmosphere. After cooling to room temperature, the yellow precipitate was collected by filtration. The precipitate was washed multiple times with methanol and then hexane to yield **6** as a yellow solid (0.1 g, 48%). ^{1}H NMR (400 MHz, THF-*d8*) δ: 9.01 (s, 4H), 8.65 (s, 2H), 8.41 (s, 4H), 8.19 (d, J = 7.6 Hz, 4H), 8.04 (s, 4H), 8.01 (s, 4H), 7.6 (t, J = 7.8 Hz, 2H), 4.27 (t, J = 6.2 Hz, 8H), 4.13 (s, 12H), 1.94 (m, 8H), 1.32 (m, 72H), 0.9 (t, J = 6 Hz, 12H); ^{13}C NMR (100 MHz, THF-*d8*) δ:, 161.4, 153.3, 151.2, 142.2, 139.0, 131.6, 131.1, 129.9, 129.3, 125.5, 125.0, 117.4, 109.0, 106.5, 70.4, 56.8, 33.0, 30.85, 30.7, 30.5, 27.4, 23.7, 14.5; MALDI-TOF MS: calcd for $C_{104}H_{136}N_4O_8$: 1570.21, found: 1570.21; anal. calcd for $C_{104}H_{136}N_4O_8$: C, 79.55; H, 8.73; N, 3.57. Found: C, 78.27; H, 8.45; N, 3.42.

QM energy calculations

The model structures (ethoxy analogs) of $\mathbf{3_i}$, $\mathbf{3_o}$, $\mathbf{3_{io}}$, $\mathbf{6_i}$, $\mathbf{6_o}$, and $\mathbf{6_{io}}$ were built in Maestro and were minimized with the OPLS force field using the MacroModel software in the Schrödinger software suite.[17] The DFT B3LYP[18] functional method with the 6-31G** basis set was employed to calculate the QM energy using the Jaguar package in the Schrödinger software. The accuracy level of SCF was selected to its highest level (fully analytic). Due to the large number of atoms in the model compounds, the STO-3G level of theory was used for minimization, followed by single point energy calculations.

Acknowledgements

We thank the National Science Foundation (DMR 0804158) and the Army Research Office (W911NF-10-1-0476) for supporting this work.

Notes and references

1 (*a*) W. Zhang and J. S. Moore, *Angew. Chem., Int. Ed.*, 2006, **45**, 4416; (*b*) M. J. MacLachlan, *Pure Appl. Chem.*, 2006, **78**, 873; (*c*) C. Ma, A. Lo, A. Abdolmaleki and M. J. MacLachlan, *Org. Lett.*, 2004, **6**, 3841; (*d*) C. S. Hartley and J. S. Moore, *J. Am. Chem. Soc.*, 2007, **129**, 11682; (*e*) S. Klyatskaya, D. Dingenouts, C. Rosenauer, B. Müller and S. Höger, *J. Am. Chem. Soc.*, 2006, **128**, 3150; (*f*) S. Höger, *Pure Appl. Chem.*, 2010, **82**, 821; (*g*) R. R. Tykwinski, M. Gholami, S. Eisler, Y. Zhao, F. Melin and L. Echegoyen, *Pure Appl. Chem.*, 2008, **80**, 621.

2 (*a*) D. Zhao and J. S. Moore, *J. Org. Chem.*, 2002, **67**, 3548; (*b*) S. H. Seo, T. V. Jones, H. Seyler, J. O. Peters, T. H. Kim, J. Y. Chang and G. N. Tew, *J. Am. Chem. Soc.*, 2006, **128**, 9264; (*c*) W. Pisula, M. Kastler, C. Yang, V. Enkelmann and

K. Müllen, *Chem.–Asian J.*, 2007, **2**, 51; (*d*) S. Chen, Q. Yan, T. Li and D. Zhao, *Org. Lett.*, 2010, **12**, 4784.
3 (*a*) M. D. Watson, A. Fechtenkötter and K. Müllen, *Chem. Rev.*, 2001, **101**, 1267; (*b*) S. Grimme, *Angew. Chem., Int. Ed.*, 2008, **47**, 3430; (*c*) D. Adam, P. Schuhmacher, J. Simmerer, L. Haussling, K. Siemensmeyer, K. H. Etzbachi, H. Ringsdorf and D. Haarer, *Nature*, 1994, **371**, 141.
4 (*a*) W. Pisula, X. Feng and K. Müllen, *Chem. Mater.*, 2011, **23**, 554; (*b*) B. R. Kaafarani, *Chem. Mater.*, 2011, **23**, 378.
5 (*a*) T. Naddo, Y. Che, W. Zhang, K. Balakrishnan, X. Yang, J. Zhao, J. S. Moore and L. Zang, *J. Am. Chem. Soc.*, 2007, **129**, 6978; (*b*) L. Zang, Y. Che and J. S. Moore, *Acc. Chem. Res.*, 2008, **41**, 1596; (*c*) W. Zhao, Q. Tang, H. S. Chan, J. Xu, K. Y. Lo and Q. Miao, *Chem. Commun.*, 2008, 4324–4326; (*d*) S. Sergeyev, W. Pisula and H. Geerts, *Chem. Soc. Rev.*, 2007, **36**, 1902–1929; (*e*) B. Walker, C. Kim and T. -Q. Nguyen, *Chem. Mater.*, 2011, **23**, 470–482.
6 (*a*) S.-H. Jung, W. Pisula, A. Rouhanipour, H. J. Räder, J. Jacob and K. Müllen, *Angew. Chem., Int. Ed.*, 2006, **45**, 4685; (*b*) W. Huang, M. Wang, C. Du, Y. Chen, R. Qin, L. Su, C. Zhang, Z. Liu, C. Li and Z. Bo, *Chem.–Eur. J.*, 2011, **17**, 440; (*c*) W. Zhang, H.-M. Cho and J. S. Moore, *Org. Synth.*, 2007, **84**, 177; (*d*) W. Zhang and J. S. Moore, *J. Am. Chem. Soc.*, 2004, **126**, 12796; (*e*) H. Wettach, S. Höger, D. Chaudhuri, J. M. Lupton, F. Liu, E. M. Lupton, S. Tretiak, G. Wang, M. Li, S. De Feyter, S. Fischer and S. Förster, *J. Mater. Chem.*, 2011, **21**, 1404; (*f*) B. N. Boden, A. Abdolmaleki, C. T.-Z. Ma and M. J. MacLachlan, *Can. J. Chem.*, 2008, **86**, 50; (*g*) J. Kaleta and C. Mazal, *Org. Lett.*, 2011, **13**, 1326.
7 Y. Che, X. Yang, Z. Zhang, J. Zuo, J. S. Moore and L. Zang, *Chem. Commun.*, 2010, **46**, 4127.
8 D. Wang, J. Hsu, M. Bagui, V. Dusevich, Y. Wang, Y. Liu, A. J. Holder and Z. Peng, *Tetrahedron Lett.*, 2009, **50**, 2147.
9 (*a*) M. Bagui, J. S. Melinger, S. Chakraborty, A. Keightley and Z. Peng, *Tetrahedron*, 2009, **65**, 1247; (*b*) M. Bagui, T. Dutta, S. Chakraborty, J. S. Melinger, H. Zhong, A. Keightley and Z. Peng, *J. Phys. Chem. A*, 2011, **115**, 1579.
10 (*a*) C. Chou, D. Wang, M. Bagui, J. Hsu, S. Chakraborty and Z. Peng, *J. Lumin.*, 2010, **130**, 986; (*b*) C. Chou, D. Wang, J. Hsu, Y. Liu and Z. Peng, *Synth. Met.*, 2009, **159**, 1657.
11 J. Kang, D. Wang, M. Bagui, S. Chakroborty and Z. Peng, *Lett. Org. Chem.*, 2006, **3**, 674.
12 C. Long, J. Kim, T. Ishizuka, Y. Honsho, A. Saeki, S. Seki, H. Ihee and D. Jiang, *J. Am. Chem. Soc.*, 2009, **131**, 7287.
13 Very weak NOE contacts between H2, H1 are also observed, indicating the existence of some minor $\mathbf{3_i}$ conformer (Fig. S5†).
14 Y. Che, X. Yang, G. Liu, C. Yu, H. Ji, J. Zuo, J. Zhao and L. Zang, *J. Am. Chem. Soc.*, 2010, **132**, 5743.
15 J.-L. Brédas, D. Beljonne, V. Coropceanu and J. Cornil, *Chem. Rev.*, 2004, **104**, 4971.
16 J. Wu, W. Pisula and K. Müllen, *Chem. Rev.*, 2007, **107**, 718.
17 Protein Preparation Wizard, Maestro, MacroModel, Phase, Induced Fit, Jaguar, and Glide; Schrödinger, LLC: Portland, OR, 2009.
18 (*a*) B. G. Johnson, P. M. W. Gill and J. A. Pople, *J. Chem. Phys.*, 1993, **98**, 5612; (*b*) C. Lee, W. Yang and R. G. Parr, *Phys. Rev. B*, 1988, **37**, 785; (*c*) A. D. Becke, *J. Chem. Phys.*, 1993, **98**, 1372.